D6.2 Localisation accuracy benchmark test for RF holography and prototype

Quanfeng Wang, Alexander Paulus, Thomas Eibert

Grant Agreement Number	101099491
Action Acronym	HOLDEN
Action Title	Ethical Design of Holography with Dense wireless Networks (HOLDEN)
Funding Scheme	HORIZON-EIC-2022-PATHFINDEROPEN-01
Version date of the Annex I against which the assessment will be made	13/12/2022
Start date of the project	1/6/2023
Due date of the deliverable	31/05/2025
Actual date of submission	30/05/2025
Responsible	TUM
Contributors	TUM
Dissemination level	Public

European Innovation Council

Funded by the European Union

Funded by the European Union. Views and opinions expressed are, however, those of the author(s) only and do not necessarily reflect those of the European Union or European Innovation Council and SMEs Executive Agency (EISMEA). Neither the European Union nor the granting authority can be held responsible for them. Grant Agreement No: 101099491.

Authors in alphabetical order

Full Name	Organisation	E-mail
Quanfeng Wang	TUM	quanfeng.wang@tum.de
Alexander Paulus	TUM	a.paulus@tum.de
Thomas Eibert	TUM	eibert@tum.de

Change History

Version	Date	Status	Author (Company)	Description
1.0	19.05.2025	Final	TUM	First final version

Executive Summary

With the advancement of wireless communication technologies and the widespread use of portable electronic devices, radio frequency (RF)-based indoor localization has gained considerable attention. A privacy-compliant indoor localization approach utilizing the 3D near-field (NF) passive radar holographic scheme presented in deliverable D3.2 has been introduced in D3.5. The concept and preliminary designs of passive tags for localization and identification have been presented, where their imaging and localization performance has been validated through both simulations and experimental measurements.

In this deliverable, the localization accuracy of the holographic scheme is analysed, with additional examples provided for imaging both unlabelled objects and passive tags. Furthermore, in response to concerns and potential opportunities identified by project partners in the ethics status monitor (ESM) [1], the holographic scheme has been extended to support data-reduced measurements, thereby enhancing its compliance with ethical and privacy considerations. An advanced passive tag design is proposed for use within the data-reduced scheme, with particular emphasis on its frequency-resonant behaviour. This pre-characterized frequency response enables accurate localization of the tags while avoiding the imaging of sensitive, labelled targets of interest (TOIs). The advantages and limitations of the proposed localization scheme are evaluated within a comprehensive evaluation framework and benchmarked against the current state of the art.

The work presented here is related to mitigation techniques for risk R1, as identified in the data protection impact assessment (DPIA) [2]. Risk R1 states that, as measurement acquisition and image generation become increasingly rapid, the associated imaging algorithms raise ethical concerns. The data used in this study includes simulations based on gender-neutral human phantoms, as well as measurement data collected in a mock-up office environment without the presence of humans. Nonetheless, the resulting findings are applicable to real-world scenarios, including those involving humans or other living beings, where privacy-sensitive considerations are critical.

The following contents are covered:

- Short introduction of the HOLDEN project and the collaboration partners
- Localization accuracy assessment for both unlabelled objects and passive tags in 3D space
- A data-reduced localization scheme, including an illustrative example featuring a novel passive tag design
- Evaluation and benchmarking of the proposed scheme against competitive state-of-the-art solutions

Table of Contents

Abbreviations

Abbreviation	Description
3D	three-dimensional
Aalto	Aalto University
CNR	Consiglio Nazionale Ricerche
DPIA	Data Protection Impact Assessment
EC	European Commission
EM	electromagnetic
ESM	Ethics Status Monitor
EU	European Union
HE	Horizon Europe
HOLDEN	Ethical design of holography in dense wireless networks
NF	near-field
PEC	perfect electric conductor
RCS	radar cross section
RF	radio frequency
RFID	radio frequency identification device
TOI	target of interest
TUM	Technical University of Munich
TWE	University of Twente
UWB	ultra-wideband
WP	work package

1. Introduction

1.1. About HOLDEN

The ubiquitous perception by sensing of objects, subjects and gestures is a pivotal challenge for future technology: it enables personalized services such as smart living, automated logistics or interaction through free-space gestures. However, it also challenges ethical and moral boundaries and threatens privacy. HOLDEN proposes a radically new approach to perception by concisely analysing ethical constraints and privacy risks while re-thinking RF-based sensing. We establish necessary conditions for privacy preserving and ethically compliant sensing and develop new paradigms respecting these constraints.

For the first time ever, HOLDEN constitutes a concentrated effort to explore social aspects of RF-sensing to guide the technological advance and to derive technology for ethically and privacy compliant perception. Central to HOLDEN is the development of ethical and privacy constraints. We use these findings to derive privacy and ethically compliant concepts for RF-based perception. We will develop a system of distributed multi-antenna devices for simultaneous multitarget recognition and ubiquitous perception with unprecedented accuracy, which constitutes a radical paradigm shift from a technology-centric perspective to a privacy-centric one via privacy by design.

HOLDEN achieves this goal along three high risk, complementary, and privacy-centric paths:

Path 1: Continuous-space measurement points: Radio-based 3D vision by holographic image processing of RF wavefronts.

Path 2: Discrete-space measurement points: Advanced 3D beamforming for human-scale recognition and tracking through dense massive connected antenna arrays.

Path 3: Signal processing and learning: High-dimensional tensor processing for the distinction of complex activities and motion from massive-dimensional RF data. The resulting breakthrough approaches and algorithms will be compared against application-level benchmarks via usage scenarios in the fields of logistics, smart living, and free-space

1.2. Partners

The consortium consists of four academic partners and a high-tech SME partner: (a) Aalto University (AALTO), Finland, (b) Technical University of Munich (TUM), Germany, (c) Consiglio Nazionale Ricerche (CNR), Italy, (d) University of Twente (TWE), Netherlands, and (e) Adant (Adant), Italy. This consortium features the specialized and complementary expertise required to achieve the project objectives. AALTO will be responsible for the project management (WP1), covered by an experienced and dedicated project manager. Ethical aspects (WP2), will be addressed by TWE (Prof. Ciano Aydin) who is a pioneer in the field. In particular, eventual gender differences in the ethical perception will be taken into account. TUM pioneered RF holography, which makes TUM (Prof. Thomas Eibert) the ideal leader of WP3. In advanced distributed signal and information processing, CNR has through Prof. Stefano Savazzi and Vittorio Rampa more than 14 years of

experience. CNR will lead WP4. Since more than 10 years, AALTO is active in radio sensing and machine learning based activity recognition. This expertise makes AALTO (Prof. Sigg) the ideal leader of WP5. Adant (Daniele Piazza) will contribute to the market analysis, application possibilities, and validation (WP6). Led by AALTO, dissemination with the website as one the media will be addressed by all partners. All academic partners are committed to early publication of results, e.g., via arXiv (open science).

2. Localization Accuracy in Holographic Schemes

2.1. Localization Accuracy of Unlabelled Objects and Passive Tags

The indoor localization technique is based on the 3D holographic imaging algorithm presented in D3.2. This method can be regarded as a hybrid approach combining RF-based and vision-based indoor localization. The concept of passive tags is introduced in D3.5. Passive tags can cause stronger scattered fields from the target of interest (TOI), which enhance localization performance. This enhancement is particularly valuable in scenarios with limited imaging resources, such as restricted observation areas or narrow signal bandwidths. Passive tags do not require batteries and they do not need to extract energy from the incident fields, which relieves the range limitations encountered with passive RF identification device (RFID) tags. In addition, the non-optical nature of the microwave images drastically reduces ethical concerns, while operation of the system does not require a visually bright illumination, which is commonly associated with and required by optical cameras.

The accuracy of the localization method is of course limited by the holographic imaging technique. As referenced in D3.5, the theoretical resolution of the imaging algorithm for typical planar observations is estimated as [5]

$$\delta_x = \frac{\lambda_c y_0}{L_x}, \quad \delta_z = \frac{\lambda_c y_0}{L_z}, \quad \text{and } \delta_y = \frac{c_0}{B}, \tag{2.1}$$

where L_x and L_y denote the aperture size and B is the bandwidth. λ_c represents the wavelength at the centre frequency and c_0 is the speed of light. y_0 is the range distance between the image plane and the observation aperture.

The purpose of the passive tags is twofold. First, the strongly scattering tags act as reliable beacons, particularly when the static TOIs are too weak to be detected or are absent from the resulting images, such as after background subtraction is applied to suppress dominant clutter in indoor environments. Second, the tags enable straightforward incorporation of various geometric features, which can be leveraged for identification purposes. However, when the scattering fields from an unlabelled TOI are strong enough, it is already possible to observe and localize the unlabelled TOI. For instances, according to the dielectric parameters of human body in [6], the interaction between the human body and electromagnetic waves in the WiFi frequency band is to a large degree characterized by reflection. As shown in Fig. 1, a simulation was carried out using the commercial full-wave simulation software FEKO [7], The body tissue is assumed to consist primarily of muscle, and the corresponding electromagnetic parameters, such as relative permittivity and dielectric loss tangent are obtained from [6]. The human body model was illuminated by plane waves at 2.4 GHz with unit amplitude incident from the front. Two near-field observation sagittal planes were used to analyse the model, one perpendicular and one parallel to xy-plane. The resulting near-field distributions are shown in Fig. 2, where significant reflections from the human body are observed.

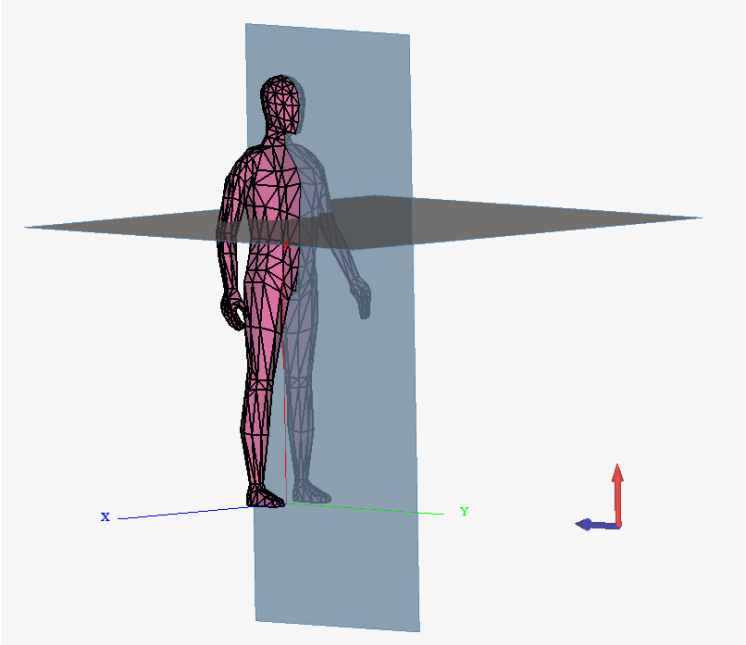

Fig. 1. Configuration of a human body illuminated by plane waves from the front. Two near-field observation planes are used to analyse the model.

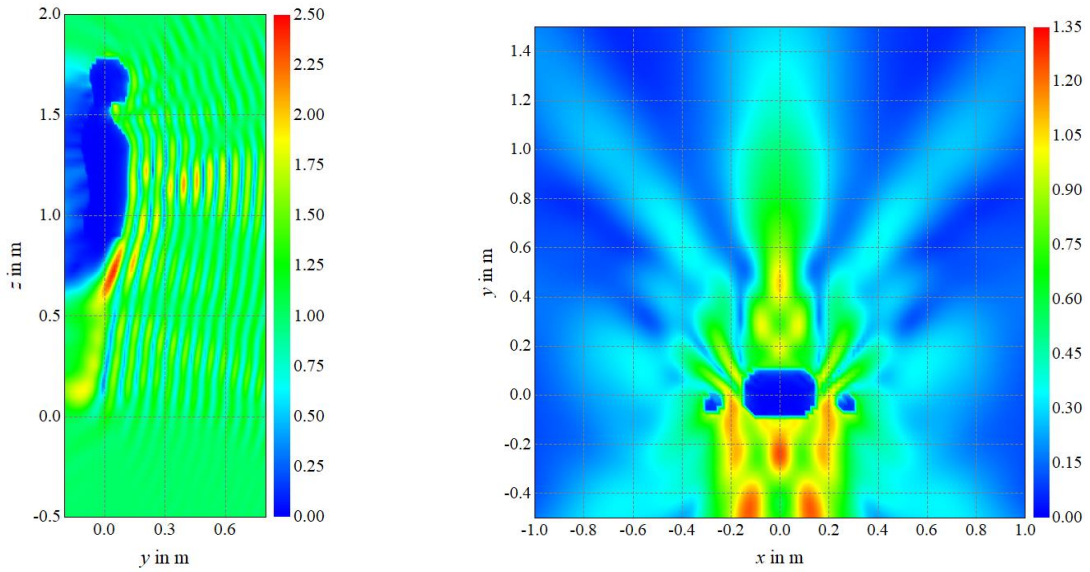

(a) (b)

Fig. 2. Simulation results of the near-field measurements in two different cut planes. (a) The plane perpendicular to the xy-plane. (b) The plane parallel to the xy-plane.

When planar near-field (NF) measurements and holographic imaging techniques are applied to the human body, the unlabelled body can already be visualized in the resulting images, provided that the scattering fields are captured with sufficient strength, and the aperture size and bandwidth are large enough to ensure adequate resolution. Using the same simulation setup as in D3.5, a Hertzian dipole located at the coordinates $x = 0$ m, $y = 2$ m, $z = 1$ m, is used as the illuminating source.

The x- and z-components of the electric field were collected over a rectangular aperture in the plane $y = 0.5\ \mathrm{m}$ extending from $x = -3\ \mathrm{m}$, $z = -3\ \mathrm{m}$ to $x = 3\ \mathrm{m}$, $z = 3\ \mathrm{m}$, positioned directly in front of the human body to capture more scattered fields. Overall, $12\,100$ uniformly distributed probe positions on the measurement plane are sampled to fulfil the minimum sampling requirement and ensure a proper resolution of the image. The imaging result of the unlabelled human body using linearly spaced frequencies from 2 GHz to 4 GHz with a step size of 50 MHz is shown in Fig. 3(a). In this case, the mannequin is clearly visible, enabling accurate localization based on the resulting image. When the frequency range is increased to 6 GHz to 8 GHz, while maintaining the same step size and all other experimental parameters, an approximately three times better resolution is achieved. As a result, a sharper image is obtained, as shown in Fig. 3(b), which potentially allows for more precise determination of positions, particularly for smaller body parts such as the hands and feet.

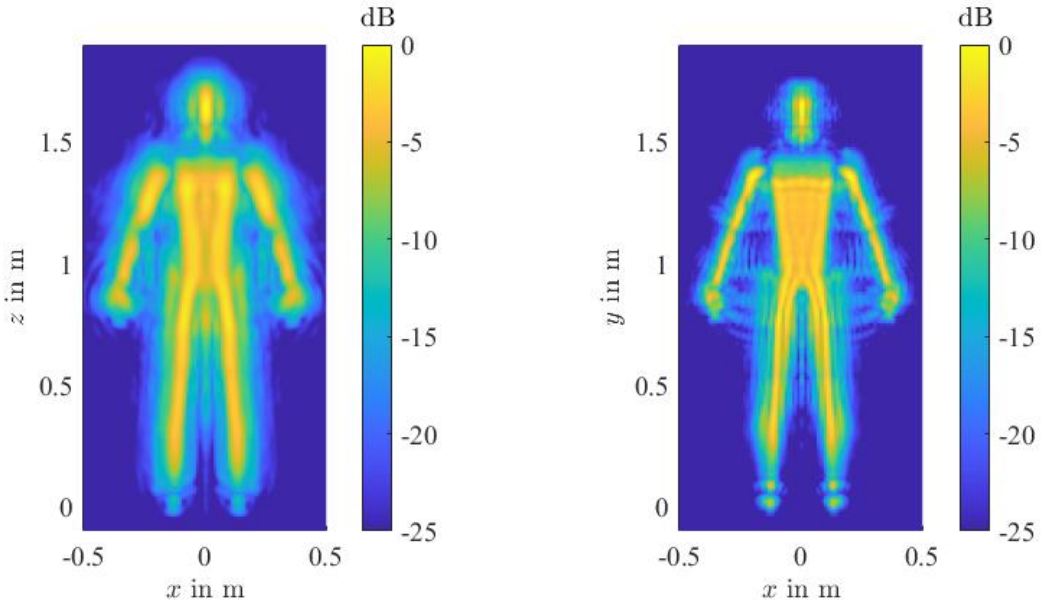

Fig. 3. Maximum intensity projection of front view for multi-frequency imaging results of the human body with a passive tag obtained by the imaging algorithm in D3.2. (a) 2 GHz to 4 GHz with a step size of 50 MHz, (b) 6 GHz to 8 GHz with a step size of 50 MHz.

In contrast, if the unlabelled objects are not strong scatterers, it may be difficult to image or localize them. For instance, as shown in Fig. 4, a wooden chair and a wooden desk serve as the TOIs. The frequency-dependent relative permittivity $\grave{o}_r$ and dielectric loss tangent $\tan\delta$ of the concrete wall, e.g., $\grave{o}_r = 2.2$ and $\tan\delta = 0.23$ at 2.21 GHz, are directly loaded from the material library of FEKO. For comparison, two perfect electric conductor (PEC) objects (that are introduced as passive tags in D3.5) are positioned above the TOIs. Using the same planar NF measurement configuration as in the previous example, and setting the frequency range from 2 GHz to 4 GHz with a step size of 50 MHz, the imaging results shown in Fig. 5 are obtained. In this case, the scattered fields from the wooden objects are significantly weaker compared to those from the PEC objects and the

mannequin in the previous example, leading to insufficient localization performance. However, with the aid of the passive tags, accurate localization becomes feasible.

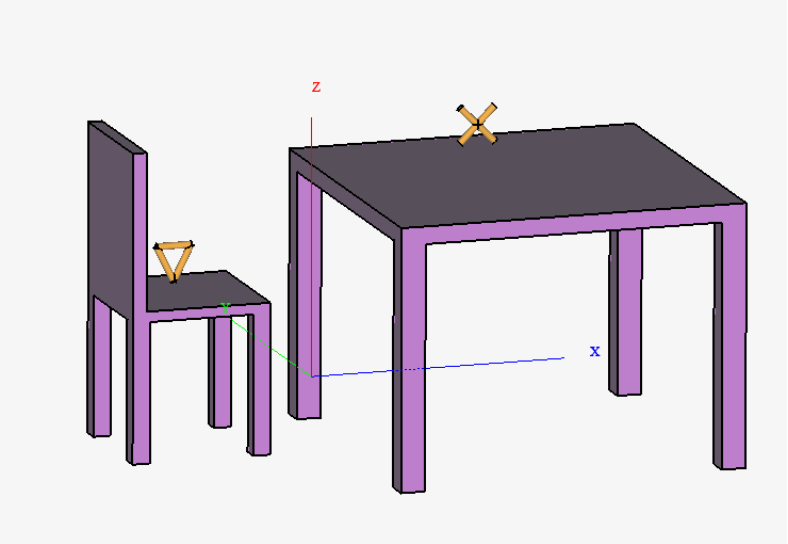

Fig. 4. Illustration of the simulation setup in FEKO, including a wooden chair and a wooden desk. Two PEC objects, which may serve as passive tags, are positioned above them.

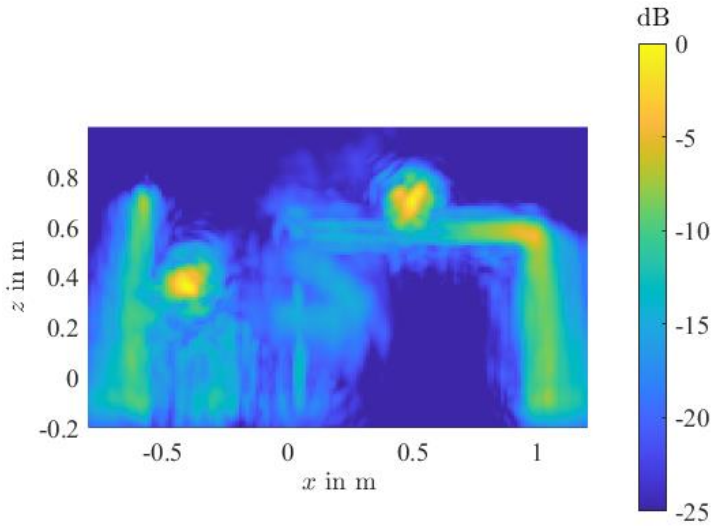

Fig. 5. Multi-frequency imaging results of the desk and chair with two PEC objects.

2.2. Comparison with the State of the Art

A comprehensive evaluation framework for localization systems is proposed in [3], which compares techniques in terms of availability, cost, energy efficiency, scalability, localization accuracy, reception range, and latency. The presented technique demonstrates advantages in terms of availability, since it is based on the concept of passive radar, which does not require complex infrastructure aside from the measurement devices. The method can be deployed conveniently in

Table I Comparison of localization techniques

	Typ. Indoor accuracy	Outdoor usable?	External or internal sensors?	Device-free?	Through-the-wall?	In the dark?
Holographic WiFi Imaging	≈ 10 cm	Yes	External, e.g., walls/ceiling	Possible	Performance deteriorates	Yes
Optical/Camera-based Tracking (OptiTrack/Vicon) [9]	Up to ± 0.2 mm	Possible	External, cameras on ceiling/walls	No	No	Yes
Laser-based Tracking / Lighthouse System (HTC VIVE Tracker 3.0) [10], [11], [12]	≈1 mm (static) ≈2 cm (dynamic)	Deteriorated performance	External+internal, laser sources on walls/ceiling	No	No	Yes
Optical+Acceleration Sensors (HTC VIVE Ultimate Tracker) [13]	typ. ≈ 3 mm (movement in cm range), ≈ 3 cm (movement in 1 m range)	Impractical / fixed environment required	Only internal	No	Yes	No
RFID sensing (Litum IoT, BlueIoT) [14], [15]	Up to 10 cm	Yes	External, Bluetooth stations on walls/ceiling	No	Yes	Yes
Ultra-Wideband Sensing (Tsingoal UWB RTLS, KKM Smart Solutions) [16]	10 cm to 30 cm	Yes	External, UWB transceiver stations	No	Performance deteriorates	Yes

various application environments, including large spaces such as offices and hospitals, with presence of ubiquitous transmitting signals. In terms of cost and energy efficiency, the passive tags are highly economical and do not require a power supply or battery. These features also enhance the scalability of the approach, where the measurement devices may, however, introduce additional costs and consume some energy. Depending on the requirements and available measurement resources, the localization accuracy can be customized over a wide range, up to micro-location accuracy [4]. The passive tags also help to extend the reception range in the considered NF scenarios. While a larger reception range may reduce localization accuracy, this can be compensated by increasing the size of the measurement aperture and the utilized bandwidth, as indicated in (2.1). Regarding latency, despite the highly-efficient implementation of the imaging algorithm, real-time localization remains challenging due to the measurement process. Nonetheless, the approach presents an alternative technical route compared to existing methods, offering enhanced privacy considerations and flexible customization options.

Among existing localization techniques for indoor use, we here consider ultra-wideband technology (for example reported research in [16], commercially sold by Tsingoal or KKM Smart Solutions), state-of-the-art optical, i.e., camera-based, tracking hardware and algorithms, which can be with external sensors (OptiTrack or Vicon) [9] or solely based on internal sensors (HTC VIVE Ultimate Tracker) [13], as well as solutions based on swept lasers merging internal and external sensors (HTC VIVE Tracker 3.0) [10], [11], [12]. All of these solutions require the user to wear or carry additional devices, which is in contrast to the potential device-free operation of holographic imaging without passive tags. A similarity between these alternatives and holographic imaging based on WiFi signals is the requirement of additional hardware in the surrounding of the user who shall be tracked. In other words, all approaches, except for the HTC VIVE Ultimate Tracker, first need sensors to be mounted to the walls or surrounding of the region within objects or persons shall be localized. These technologies are based on “external” observations, i.e., they derive the location of a target

from observations made by external devices (“looking at the target from the outside”, “outside-in”), which usually leads to a high precision, however, at the inconvenience of being limited to a finite region within which the sensors have been installed. In contrast to this, “internal” sensor systems like the HTC VIVE Ultimate Tracker derive the target location in space from sensor information “looking from the target towards the outside” (“inside-out”) and, thus, are usually more flexible. However, deriving location information with an “outward-looking” technique is known to be less precise and more sensitive to environmental conditions than “inward-looking” methods.

A broad overview and comparison on localization technologies is given in Table I. The typically expectable localization accuracy for indoor environments is reported, as well as the applicability for outdoor use. Information on the type of sensors, i.e., external or internal, is provided, as well as the suitability of the solutions to work in the dark or through walls, i.e., when no direct line of sight is available. It can be seen that external camera-based systems currently provide the highest level of accuracy in the sub-mm range for room-scale indoor localization. Without the need to place additional sensors on the walls or ceiling of a room, the internal HTC VIVE Ultimate Tracker does provide a position accuracy in the cm range, however, which deteriorates under low-light conditions or when the region of interest increases to multiple meters. Only solutions based on RFID [14], [15], ultra-wideband (UWB) [16] or on holography potentially allow for tracking of persons or objects through walls. While considered to be less popular, the achievable tracking accuracy of UWB solutions is reported to be in the range of 10 cm to 30 cm, which could be on a similar scale to that of WiFi holography. While fully operational in the dark or outside, where the sun is likely to deteriorate the performance of camera or laser-based solutions, RFID and UWB tracking requires tags to be attached to or carried by the targets.

3. Evaluation of Reduced Data Schemes

3.1. Reduction in the Spectral Domain

For the localization algorithm in D3.5, its effectiveness and accuracy depend on the quality of imaging, which in turn relies on a certain amount of near-field measurement data. If the aperture size of the NF measurement plane is insufficient or the frequency bandwidth is too narrow, which leads to reduced cross-range and range resolution, the imaging performance will significantly deteriorate. However, if the focus is solely on localization, it is possible to arrive at a reduced data scheme. With the aid of the powerful inverse source reconstruction solver introduced in D3.2, inverse sources at multiple frequencies are efficiently and accurately reconstructed, and their frequency-domain characteristics are preserved in subsequent imaging algorithms. Considering that most objects exhibit relatively simple scattering behaviour and equivalent source frequency responses under external illumination, it becomes feasible to design uniquely identifiable frequency-response tags. By pre-measuring their spectral characteristics, one can determine the location of the passive tag by performing pixel-wise comparisons across the series of single-frequency images obtained.

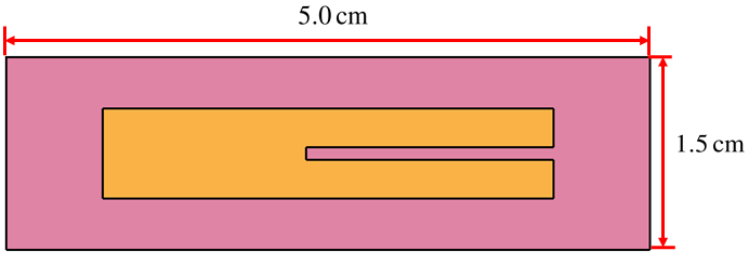

Fig. 6. Example of a coplanar-strip resonator as passive tag.

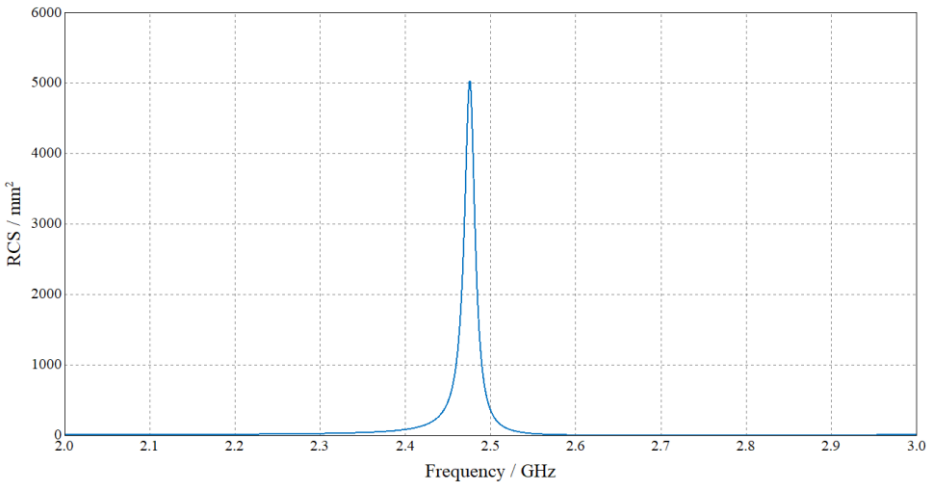

Fig. 7. Monostatic RCS of the passive tag.

One example is shown in Fig. 6, where the passive tag is based on the coplanar-strip resonator introduced in [8] and has been adapted to meet the requirements of this work. The overall dimensions of the tag are $5.0\ \mathrm{cm} \times 1.5\ \mathrm{cm} \times 0.8\ \mathrm{cm}$. It is designed on a single-layer FR-4 dielectric substrate with a relative permittivity of 4.4. Overall, the passive tag is compact and low-cost, making it suitable for practical deployment.

The passive tag is designed to resonate at 2.48 GHz. When illuminating the passive tag with plane waves with vertical polarization, the monostatic radar cross section (RCS) of the tag within the frequency range of 2 GHz to 3 GHz is shown in Fig. 7. The tag is positioned directly below the right hand of the human model for simulations, as shown in Fig. 8. In this new setup, a data-reduced scheme is considered. The simulation bandwidth is significantly narrowed, with frequencies limited to the range of 2.4 GHz to 2.5 GHz with a step size of 5 MHz. Additionally, the NF measurement aperture is reduced to half the area of that used in previous simulations, spanning from $x = -1.5\ \mathrm{m}$, $z = -0.5\ \mathrm{m}$ to $x = 1.5\ \mathrm{m}$, $z = 2.5\ \mathrm{m}$, and is positioned farther from the TOI at $y = 1.0\ \mathrm{m}$. Collectively, these changes lead to a significant reduction in spatial resolution. As expected, the resulting image under these constrained conditions is considerably degraded, as shown in Fig. 9. The image is dominated by artifacts, the outline of the mannequin is severely distorted, and the passive tag is no longer discernible.

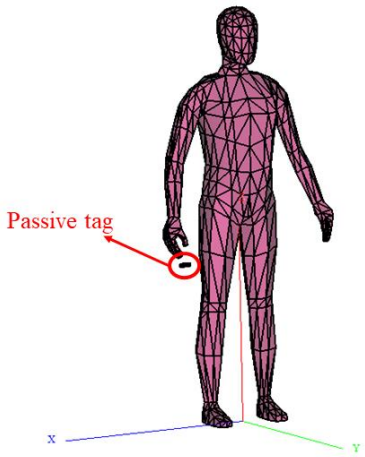

Fig. 8. Illustration of the simulation setup in FEKO including a human model and a passive tag positioned directly below the right hand of the human model.

Nonetheless, when the frequency response of the passive tag is pre-measured and, thus, known, its corresponding resonant features can still be preserved during the inverse equivalent source reconstruction process. By removing the human body model while retaining only the passive tag and keeping all simulation parameters unchanged, the multi-frequency holographic imaging results of the reconstructed equivalent sources are obtained, as shown in Fig. 10(a). It can be observed that the passive tag is still well reconstructed, although the imaging quality is not ideal

and the sidelobes are strong under the current narrow bandwidth conditions due to the point spread effect. By selecting the brightest pixel in the image which represents the most probable location of the passive tag, and examining the intensity across individual frequency points, the resulting frequency response shown in Fig. 10(b) is extracted. A similarity to the response in Fig. 7 can be clearly observed.

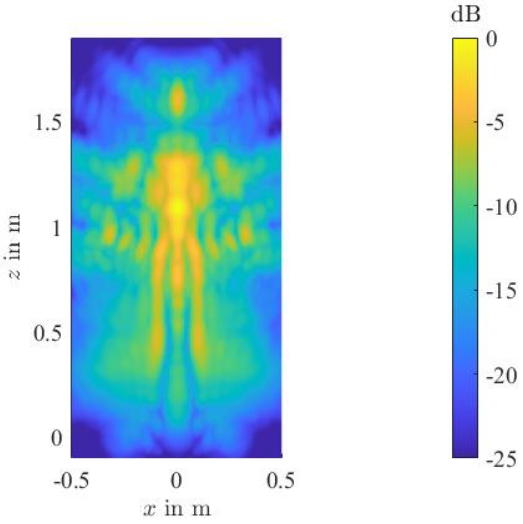

Fig. 9. Maximum intensity projection of front view for multi-frequency imaging results of the human body with the passive tag.

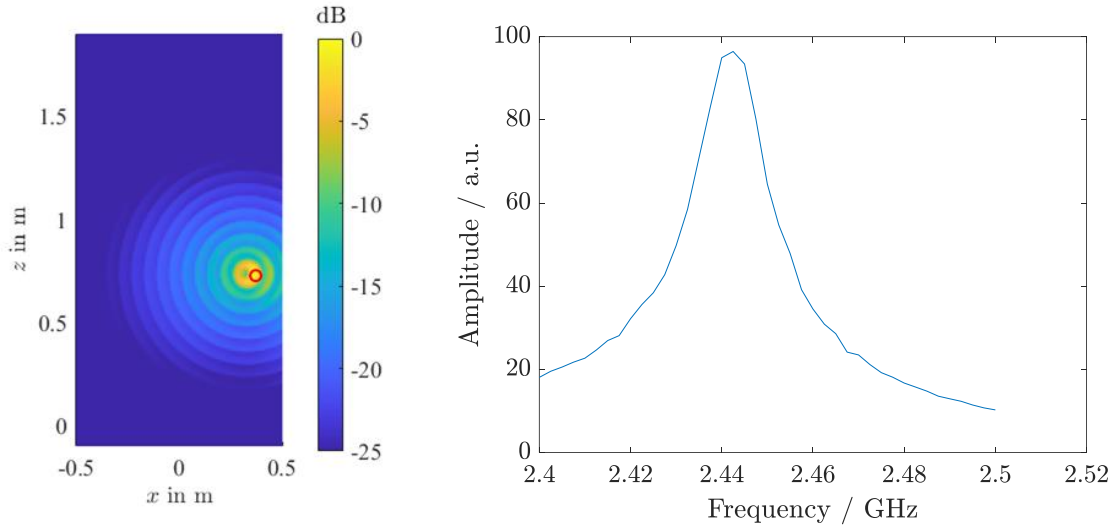

(a) (b)

Fig. 10. (a) Multi-frequency imaging results of the passive tag obtained by the imaging algorithm in D3.2. (b) Intensity of the brightness pixel (highlighted by the red circle) across individual frequency points.

Therefore, with this pre-measured frequency property on hand, the position of the passive tag can be recovered by calculating the correlation coefficient pixel by pixel with the imaging results from Fig. 9. The result is shown in Fig. 11, where a single prominent bright spot is observed in this cut-plane, and its location matches that of the passive tag. The main body of the human model disappears, leaving only minor artifacts, as the scattering characteristics of the human body differ significantly from those of the passive tag. Furthermore, this outcome aligns more closely with ethical and privacy considerations, as only the position of the passive tag is reconstructed, while other sensitive information, such as the identity or structure of the tagged object, is effectively concealed in the process.

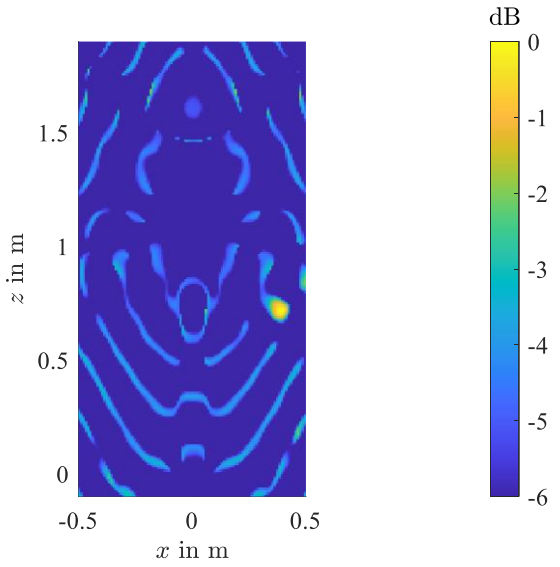

Fig. 11. Magnitudes of the correlation coefficients at cut-plane $z = 0.73$ m.

3.2. Reduction in the Spatial Domain

In a practical realization of the holographic imaging, the measurement instrumentation will not only be limited by the bandwidth of the Wi-Fi signals, however, the arrangement of the receiving antenna array will also play a crucial role. As has been reported, the number of measurement samples and the dimensions of the receiving array directly affect the achievable resolution and precision with which images are computed. As estimated by (2.2), larger receiver arrays, i.e., larger areas on which the scattered fields are recorded, lead to a better resolution. In addition, the sampling of the measurement area needs to be sufficiently dense in order to suppress aliasing artifacts that would otherwise arise.

In order to obtain an estimate of a realistically achievable resolution with Wi-Fi imaging, measurement data collected with the planar scanner, which has been described in D3.3, has been processed with artificially reduced measurement areas. Fig. 12 illustrates the test scenario where a metallic flask was placed at the two locations labelled with “A” and “E” on the desk of the office room featuring the planar scanner. By employing the difference of the two datasets, the scattering contributions from the background, i.e., from other objects and furniture within the room, are

effectively suppressed, and the locations of the bottle at point “A” and point “E” should be visible in the computed image. For the following investigation, data at a single frequency of 2.425 GHz has been utilized for image generation.

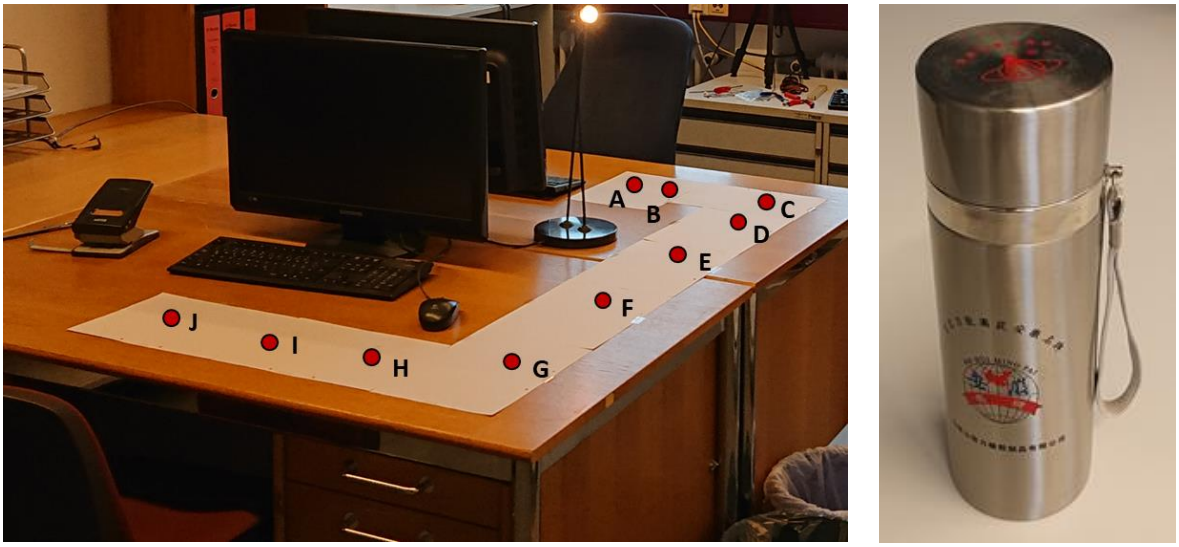

(a) (b)

Fig. 12. Test environment, (a), and test object, (b), which is placed at locations “A” and “E” in the following.

Figs. 13(a) and (b) show the maximum projections of the three-dimensional images in the xy-plane for measurement surfaces with edge lengths of around 0.5 m and 2 m. It can be observed that the two targets, i.e., the flask at the two locations “A” and “E”, cannot be differentiated when the receiver aperture is too small. Figs. 14(a) and (b) illustrate the same truncation effect for a projection in the xz-plane, which furthermore shows that not only the number of targets is wrongly estimated from a too small aperture, but also the distance of the objects in normal direction to the measurement surface is inaccurately determined. While the resolution estimate in normal direction (2.3) would be expected to go to infinity, i.e., no separation of distance could be done with data at a single frequency, the correct modelling of near-field effects allows to localize the object(s) in three-dimensional space.

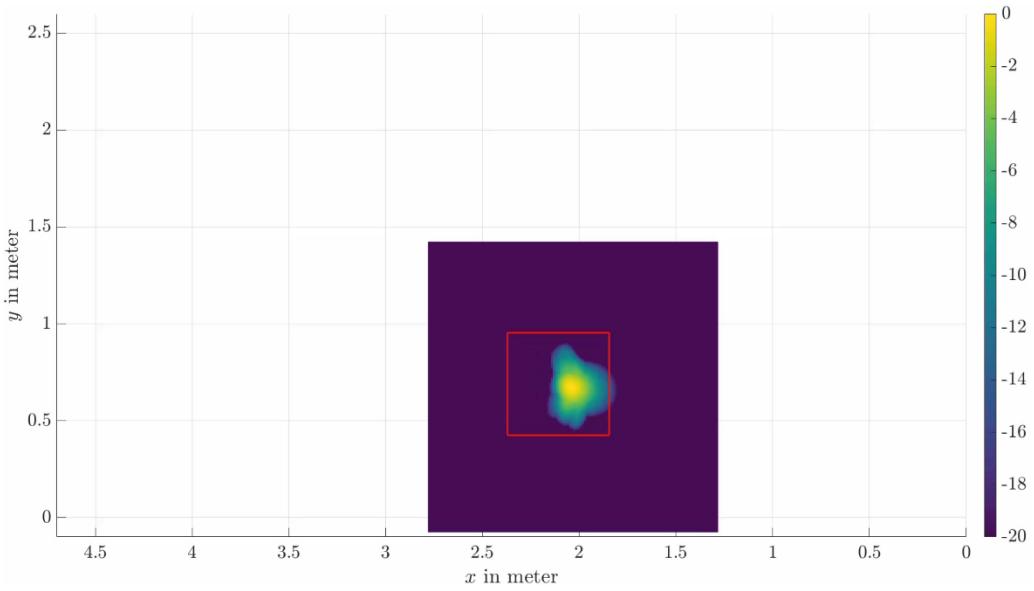

(a)

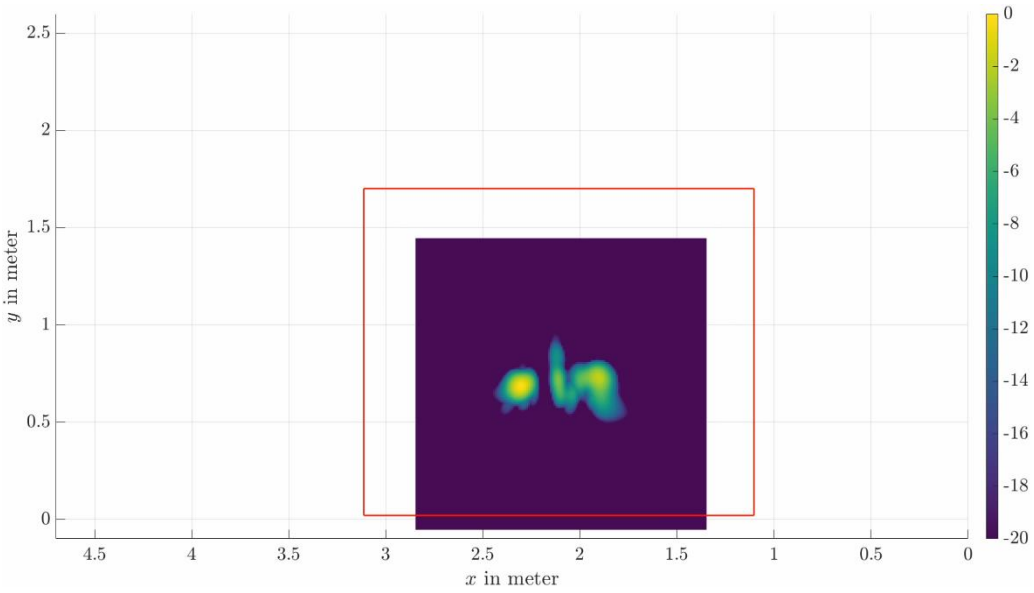

(b)

Fig. 13. Images computed from a measurement surface (indicated by the red square) of approximately $0.5\ \mathrm{m} \times 0.5\ \mathrm{m}$ (a), and approximately $2\ \mathrm{m} \times 2\ \mathrm{m}$, (b). Maximum-intensity projections to the xy-plane in dB.

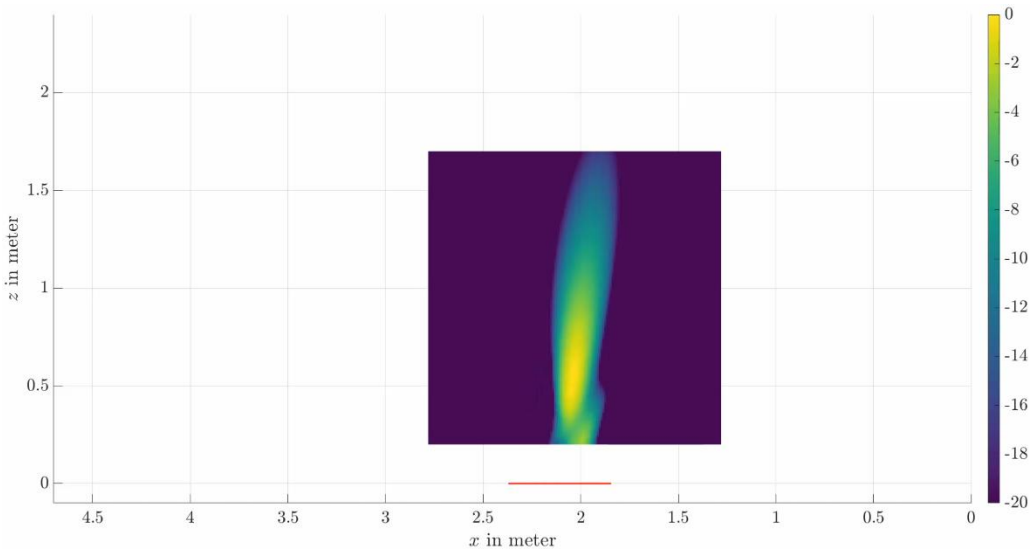

(a)

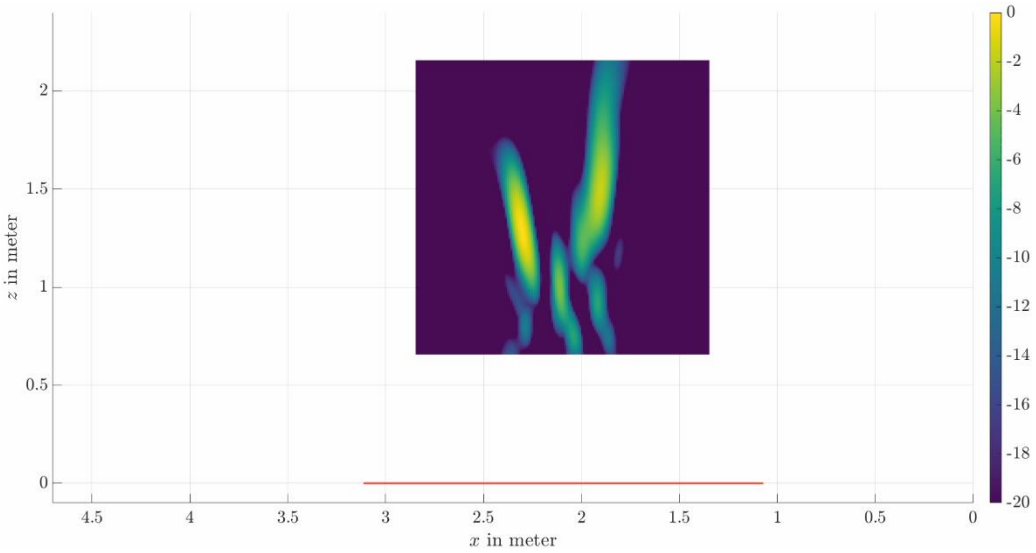

(b)

Fig. 14. Images computed from a measurement surface (indicated by the red square) of approximately $0.5\,\mathrm{m} \times 0.5\,\mathrm{m}$ (a), and approximately $2\,\mathrm{m} \times 2\,\mathrm{m}$, (b). Maximum-intensity projections to the xz -plane in dB.

4. Summary

An indoor localization method based on a 3-D holographic passive radar imaging technique has been discussed and illustrated in D3.5. In this deliverable, the localization accuracy of the indoor localization method has been evaluated, presenting simulation results for detecting unlabelled objects and passive tags. This localization method utilizes passive tags that rely solely on electromagnetic scattering and eliminate the need for traditional signal transmission or response mechanisms commonly used in technologies like RFID. The approach allows for precise localization in an intuitive manner within complex indoor geometries.

In response to ethical and privacy concerns, a spectral data-reduced localization scheme has been developed to limit the requirements of dense data collection. This includes a new passive tag design optimized for frequency-specific detection, allowing for precise localization without compromising sensitive information. The localization system is assessed within a rigorous evaluation framework and compared to current state-of-the-art technologies. Furthermore, imaging results from measurement data indicate that indeed the achievable resolution can conveniently be altered by limiting the measurement surface to smaller sized areas. As a direct consequence, the size of the receiver array always has to be chosen to fulfil the requirements by a specific application at hand – and to potentially comply with space limitations when for example targeting localization within small rooms.

5. References

[1] S.I. Cammers-Goodwin, N. Gertz, C. Aydin, T. Eibert, M. Nagenborg, S. Savazzi, S. Sigg, "D8.9 ethics status monitor (ESM) version 2", Oct. 2024, Available: https://holden-project.eu/deliverables/

[2] S. Sigg, "D8.8 – Data Protection Impact Assessment (DPIA) version 1", Apr. 2024, Available: https://holden-project.eu/deliverables/

[3] F. Zafari, A. Gkelias, and K. K. Leung, "A survey of indoor localization systems and technologies," IEEE Commun. Surv. Tutor., vol. 21, no. 3, pp. 2568–2599, 2019.

[4] F. Zafari, I. Papapanagiotou, and K. Christidis, "Microlocation for Internet-of-Things-equipped smart buildings," IEEE Internet Things J., vol. 3, no. 1, pp. 96–112, Feb. 2016.

[5] Lopez-Sanchez, J. M. and J. Fortuny-Guasch, "3-D radar imaging using range migration techniques," IEEE Trans. Antennas Propag., Vol. 48, No. 5, 728–737, May 2000.

[6] Body Tissue Dielectric Parameters: https://www.fcc.gov/general/body-tissue-dielectric-parameters, FCC, US. Accessed: 11 Oct. 2023.

[7] Altair. (2024) FEKO. [Online]. Available: https://altairhyperworks.com/product/FEKO

[8] V. Arnaud, P. Etienne, and T. Smail, "Design of Compact and Auto-Compensated Single-Layer Chipless RFID Tag," IEEE Trans. Microw. Theory Techn., vol. 60, no. 9, pp. 2913–2924, Sep. 2012.

[9] A. M. Aurand, J. S. Dufour, and W. S. Marras, "Accuracy map of an optical motion capture system with 42 or 21 cameras in a large measurement volume," J Biomech, vol. 58, pp. 237–240, Jun. 2017.

[10] S. Merker, S. Pastel, D. B¨urger, A. Schwadtke, and K. Witte, "Measurement accuracy of the HTC VIVE Tracker 3.0 compared to vicon system for generating valid positional feedback in virtual reality," Sensors, vol. 23, no. 17, p. 7371, Jan. 2023.

[11] J. Lwowski, A. Majumdat, P. Benavidez, J. J. Prevost, and M. Jamshidi, "HTC VIVE Tracker: Accuracy for indoor localization," IEEE Syst. Man Cybern. Mag., vol. 6, no. 4, pp. 15–22, Oct. 2020.

[12] M. Borges, A. Symington, B. Coltin, T. Smith, and R. Ventura, "HTC VIVE: Analysis and accuracy improvement," in 2018 IEEERSJ Int. Conf. Intell. Robots Syst. IROS, Oct. 2018, pp. 2610–2615.

[13] J. Kulozik and N. Jarrass´e, "Evaluating the precision of the HTC VIVE Ultimate Tracker with robotic and human movements under varied environmental conditions," Sep. 2024, arXiv, doi:10.48550/arXiv.2409.01947.

[14] D. R. Philips, E. Salami, H. Ramiah, and J. Kanesan, "Location accuracy optimization in bluetooth low energy (BLE) 5.1-based indoor positioning system (IPS)—a machine learning approach," IEEE Access, vol. 11, pp. 140 186–140 201, 2023.

[15] A. Ülkü, "The next generation in personnel/people tracking: Active RFID technology has allowed for enhanced security and safety," IEEE Consum. Electron. Mag., vol. 6, no. 4, pp. 122–124, Oct. 2017.

[16] M. Dong, Y. Qi, X. Wang, and Y. Liu, “A non-line-of-sight mitigation method for indoor ultra-wideband localization with multiple walls,” IEEE Trans. Ind. Inform., vol. 19, no. 7, pp. 8183–8195, Jul. 2023.

6. Table of Figures and Tables